

Journal Pre-proof

Noncovalent interaction stabilizes the 2,4-Dinitrophenylhydrazone Derivatives over g-C₃N₄ surface to enhance optical properties: Synthesis, characterization, and DFT investigation

Mohammed T. Alotaibi

PII: S0022-2860(20)30517-2

DOI: <https://doi.org/10.1016/j.molstruc.2020.128192>

Reference: MOLSTR 128192

To appear in: *Journal of Molecular Structure*

Received Date: 18 January 2020

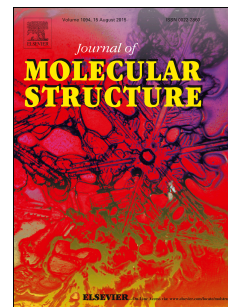
Revised Date: 31 March 2020

Accepted Date: 1 April 2020

Please cite this article as: M.T. Alotaibi, Noncovalent interaction stabilizes the 2,4-Dinitrophenylhydrazone Derivatives over g-C₃N₄ surface to enhance optical properties: Synthesis, characterization, and DFT investigation, *Journal of Molecular Structure* (2020), doi: <https://doi.org/10.1016/j.molstruc.2020.128192>.

This is a PDF file of an article that has undergone enhancements after acceptance, such as the addition of a cover page and metadata, and formatting for readability, but it is not yet the definitive version of record. This version will undergo additional copyediting, typesetting and review before it is published in its final form, but we are providing this version to give early visibility of the article. Please note that, during the production process, errors may be discovered which could affect the content, and all legal disclaimers that apply to the journal pertain.

© 2020 Published by Elsevier B.V.



AUTHORSHIP STATEMENT

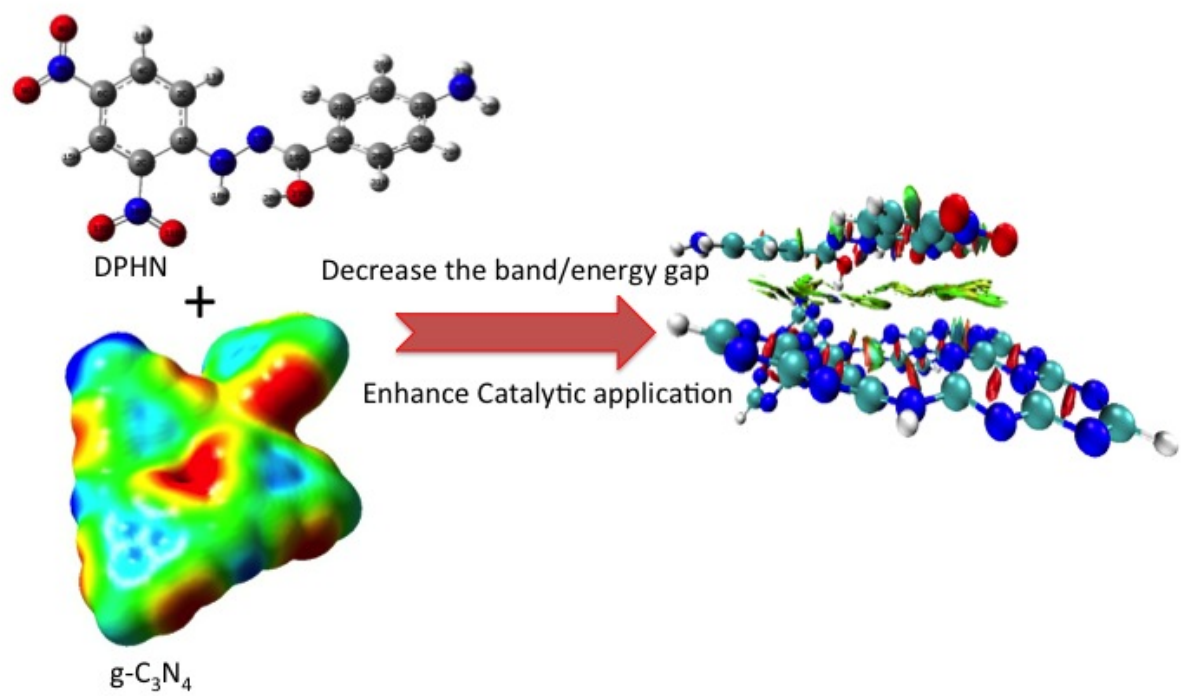
Manuscript title: Noncovalent interaction stabilizes the 2,4-Dinitrophenylhydrazone Derivatives over g-C₃N₄ Surface to Enhance Optical Properties: Synthesis, Characterization, and DFT Investigation

Authorship contribution

I hereby declare that I, Mohammed T. Alotaibi performed the Conception and design of study, acquisition of data, analysis and/or interpretation of data, Drafting the manuscript, and Approval of the version of the manuscript to be published

Author name

Mohammed T. Alotaibi



Journal

Noncovalent interaction stabilizes the 2,4-Dinitrophenylhydrazone Derivatives over g-C₃N₄ Surface to Enhance Optical Properties: Synthesis, Characterization, and DFT Investigation

Mohammed T. Alotaibi

Department of Chemistry, Turabah University collage, Taif University, Turabah, Saudi Arabia

Abstract

Immobilization of organic compounds on semiconductor surface was recently exploited to enhance the semiconductor light absorption and photocatalytic performance. Here, synthesis of 2,4-Dinitrophenylhydrazone-benzaldehyde (DPHH), 2,4-Dinitrophenylhydrazone-2-thiophenecarboxyaldehyde (DPHS), 2,4-Dinitrophenylhydrazone-4-dimethylaminobenzaldehyde (DPHN) and 2,4-Dinitrophenylhydrazone-4-aminobenzoic acid (DPHB) was introduced and characterized with different spectroscopic techniques such as FT-IR and UV-Vis spectroscopy. The UV-vis absorption spectra of the hydrazone compounds were stabilized (red shifted) in polar solvents such as N,N-dimethylformamide (DMF) and acetonitrile (ACN). Density functional theory (DFT) was used to investigate the structures conformations and stabilizing forces. Doping of g-C₃N₄ nanosheets with 5% of the hydrazone derivatives decreases the optical band gap from 2.71 eV to 2.62 eV with DPHN derivatives. The DFT investigation coupled with reduced density gradient (RDG) show that hydrazone derivatives was stabilized on g-C₃N₄ by vdW forces. These results shows that the hydrazone derivatives could be potentially used as sensitizers for photocatalysis and solar cells systems.

Keywords: 2,4-Dinitrophenylhydrazone derivatives; solvent effect; g-C₃N₄; optical bandgap; DFT

1. Introduction

Recently, photocatalysis has been emerged as promising process for different applications [1,2]. For example, harvesting sunlight by semiconductors for renewable energy production such as H₂ under visible light is a promising economic and clean technology [3]. On another hand, removal of organic/inorganic pollutants from wastewater is efficient and cheap photocatalysis applications [4,5]. In photocatalysis, semiconductor plays the vital role in light absorption and subsequent electron/hole generation process [6]. Different semiconductors materials have been used such as TiO₂ [7,8], MoS₂ [9,10], V₂O₅ [11], and g-C₃N₄ [6,12]. The metal free 2D dimension g-C₃N₄ is one of the promising materials in these applications. The structure of g-C₃N₄ has been theoretically investigated by different researchers [13-16]. The corrugated structure was more stable than the corresponding planar isomer, which stabilizes the Fermi level and increasing the active site through π -hole formation [13,14]. The mechanical properties of g-C₃N₄ such as strain response, elastic constant electronic and magnetic properties was explored [17,18]. The electric properties of the nanosheet was stable under 10 V/nm electric field. However, the pristine g-C₃N₄ material suffers from different drawback such as the lack of visible light absorption and the fast electron/hole recombination. In order to overcome these drawbacks, several techniques have been used such as doping g-C₃N₄ with metal nanoparticles [19,20] to prevent the electron/hole recombination process or with organic dyes to extend the visible light absorption efficiency. To increase the g-C₃N₄ visible light absorption, several dyes have been used such as Montmorillonite [21], Bentonite [22], Erythrosine B [23], Fluorescein [19,24], Eosin Y, basic fuchsin [25] and Rose Bengal

[26]. However, most of the used dyes suffer from stability, expensive, and in some cases the tedious preparation method.

On the other hand, 2,4-dinitrophenylhydrazine (2,4 DNP) reacts with different aldehydes and ketones by condensation reactions to give the corresponding hydrazone compounds in high yield and moderate conditions [27-29]. The reaction results on colored compounds, which is the basis for the visual detections of aldehydes and ketones in vivo and vitro applications [30]. It is also used in high throughput detection of mutants strains [31]. 2,4 DNP was used in combination with nanoalumina for adsorption of heavy metals from water [32]. In addition, pyrazolone derivatives were reported as an antibacterial and anti-tuberculosis agents [33].

Here, we use the simple synthesized of 2,4 DNP hydrazone derivatives coupled with $g\text{-C}_3\text{N}_4$ to enhance the optical band gap. The synthesized compounds were characterized with different spectroscopic techniques such as FT-IR and UV-Vis in different solvents. Theoretical calculations with density functional theory (DFT) were corroborated experimental results to further investigate the titled compounds.

2. Experimental

2.1 Materials: 2,4-dinitrophenylhydrazine (2,4-DNP), 4-dimethylaminobenzaldehyde, 2-thiophenecarbaldehyde, and 4-aminobenzoic acid was purchased from Sigma-Aldrich, Germany. All solvents were supplied by Sigma-Aldrich, Germany and used without further purification.

2.2 Preparations

2,4-DNP derivatives: preparation of 2,4-DNP derivatives were performed according to the literature [28]. For example, DPHN was synthesized by taking 0.99 g (5 mmole) from 2,4-DNP and 0.745 g (5 mmole) from 4-dimethylaminobenzaldehyde in ethanol. The 2,4-DNP

color was orange which turns to deep brown after DPHN formation. The solution was refluxed for 4 h at 120 °C for complete reaction. The deep brown DPHN solid product was collected by filtration and washed with ethanol several times. Similarly, 2,4-DNP was reacted with 2-thiophene-carbaldehyde, 4-aminobenzoic acid, and benzaldehyde and the products were coded as DPHS, DPHB, and DPHH respectively.

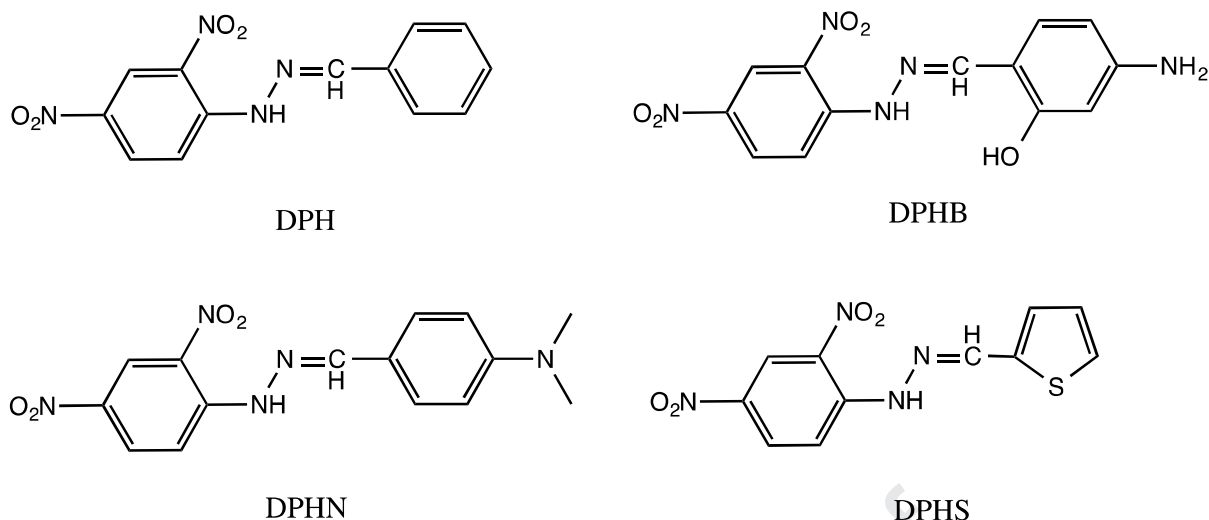
g-C₃N₄ nanosheet: the bulk g-C₃N₄ was synthesized by adding 10 g of urea in a closed crucible and heated in furnace at 550 °C for 2h (5 °C/min). g-C₃N₄ nanosheet was prepared by dissolving 100 mg of the bulk g-C₃N₄ in methanol and sonicated for 4 hrs. Then the solution was centrifuged and removed the remained solid product. The suspended g-C₃N₄ nanosheet was collected and stored for further use.

2.3 Characterization

The UV-Vis absorptions measurements of hydrazone derivatives in different solvents were performed using Perkin-Elmer Lambda 11 UV/VIS spectrophotometer using 1 cm quartz cell. Reflectance measurements were performed using Ocean optic spectrometer USB4000-UV-VIS-ES. The fluorescence measurements were performed using JASCO spectrofluorometer (model-FB-8300). IR was measured using Perkin-Elmer FT-IR spectrophotometer in 4000-400 cm⁻¹ range.

2.4 Computational details

The structures were optimized to the minimum energy using Gaussian09 package [34]. Frequency calculations were performed in order to confirm that the optimized structures have minimum energy at the potential energy scan. B3lyp functional was used with the 6-311G(d,p) basis set. Time-dependent density functional theory (TD-DFT) was performed to calculate the molecular frontier HOMO and LUMO orbitals. Non-covalent interactions (NCI) were investigated using Multiwfn program [35] and visualized by VMD (1.9) [36].



Scheme 1: structure of 2,4 DNP derivatives.

3. Results and Discussion

3.1 Structures geometry optimization of hydrazone derivatives

The reaction between 2,4 DNP and different aldehydes through condensation yields Schiff bases, DPHH, DPHS, DPHN, and DPHB (Scheme 1). The optimized structure of 2,4 DNP showed that the compound was stabilized by the strong hydrogen bonding between H18...O11 (Fig.1a). The calculated electrostatic potential shows the presence of electron deficiency region over the -NH_2 group which could be the possible position for the nucleophilic attack (Fig 1b). The condensation reactions on the NH_2 group for 2,4 DNP was confirmed by the HOMO and LUMO energy calculations (Fig.1c and d). The HOMO orbital of 2,4 DNP was distributed over the whole molecule, particularly the NH_2 group, while the LUMO orbitals was situated on the phenyl ring [37]. The reaction of 2,4 DNP with different aldehyde in ethanol yields 2,4 DNP hydrazone derivatives (Scheme 1). DFT calculations show that the products were stabilized by strong hydrogen bond (HB) between the NO_2 oxygen atom and the -N-H group hydrogen atom, which is reported for similar hydrazone compounds in solid state [38] and solution [28]. The HB distance was 1.85, 1.84, 1.85, 1.84 Å and the bond angle of 129.1, 129.8, 129.7, 129.5° for DPHH, DPHS, PDHN, and DPHB respectively (Fig. 2). DPHS and DPHN were planar molecules with dihedral angle around the N-N of 180°

[28], while the DPHH and DPHB was offset by a dihedral angle of 62.4° and 156.6° respectively.

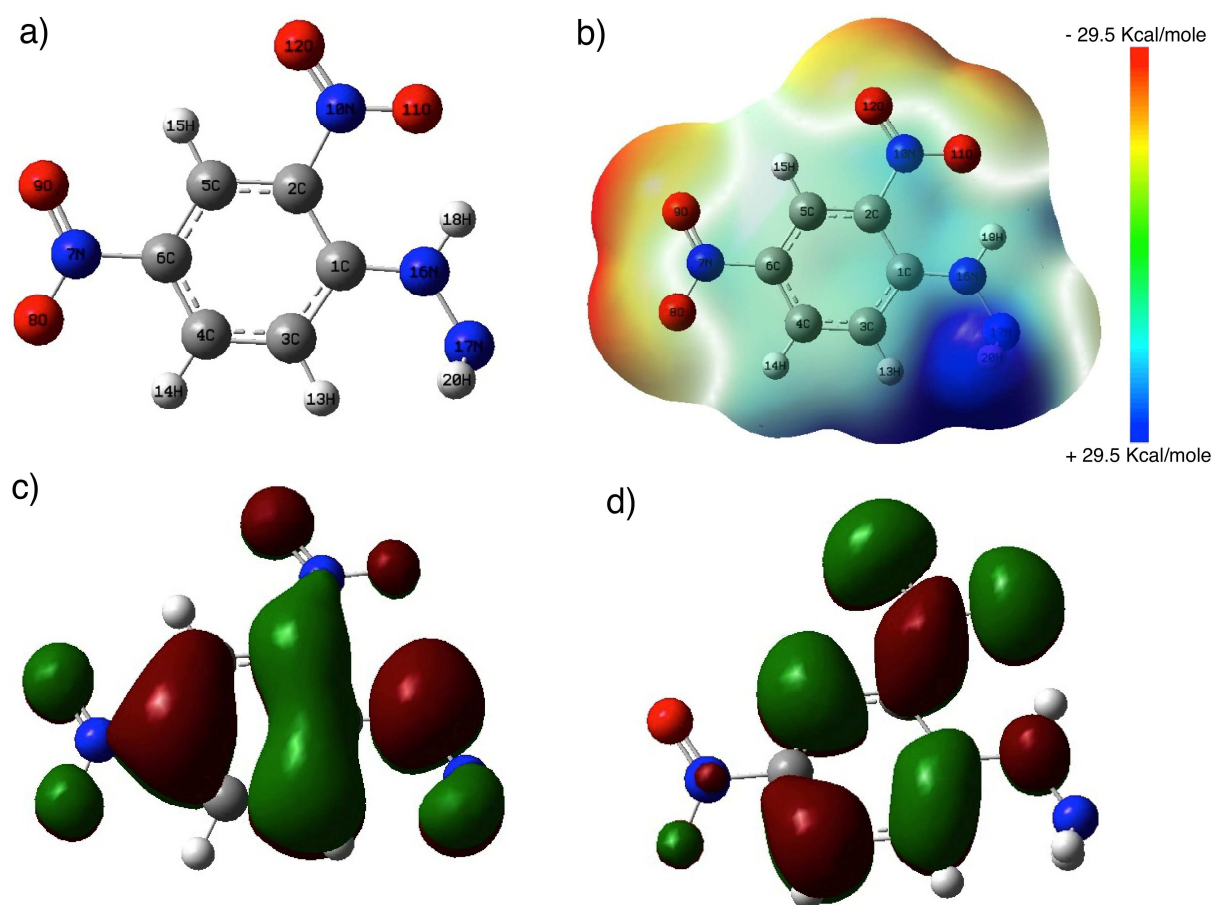


Fig.1: a) optimized 2,4-DNP structure, b) MEP of 2,4-DNP, c) HOMO orbital of 2,4-DNP, d) LUMO orbital of 2,4-DNP calculated at B3lyp/6-311g(d,p).

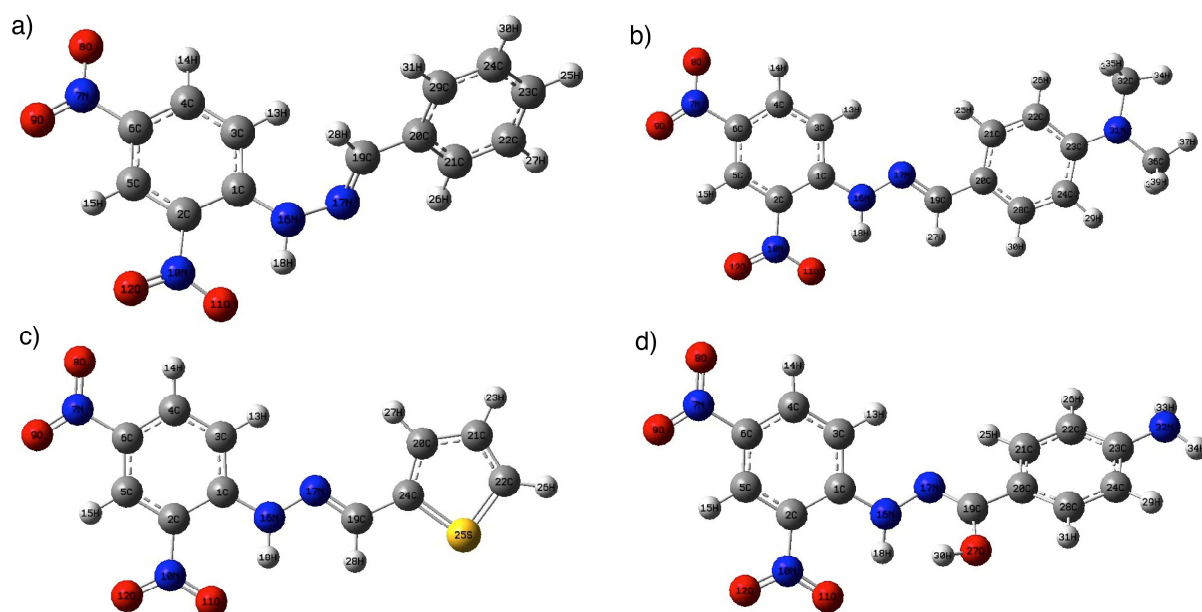


Fig.2: optimized structures of 2,4-DNP hydrazone derivatives a) DPHH, b) DPHN, c) DPHS, and d) DPHB calculated at B3lyp/6-311g(d,p).

The reaction of 2,4 DNP with different aldehyde was investigated by the FT-IR spectroscopy. 2,4-DNP shows vibration peaks at 3390 and 3300 cm^{-1} , which corresponds to the NH_2 and N-H groups respectively (Fig.3a) [28]. The C-H stretching aromatic mode for benzene ring vibration appears at 3072 cm^{-1} in addition to the in plane-bending mode (1400-850 cm^{-1}) and out of plane bending mode (950-600 cm^{-1}) (Fig.3b). In addition, 2,4 DNP has two NO_2 groups, which normally show up for free groups in the region 1600-1350 cm^{-1} for symmetric and antisymmetric stretching modes. However, in this work, the antisymmetric and symmetric modes of NO_2 observed at 1566 and 1367 respectively. The NO_2 groups vibrations were red shifted compared to the literature values (1600-1349 cm^{-1}) [39], was attributed to intramolecular hydrogen bond formation (N-H.. O_{nitro}). The in-plane and out-of plane modes of NO_2 groups appear at 827 and 620 cm^{-1} respectively. Upon reaction of 2,4-DNP with the corresponding aldehyde, for example DPHN, the peak at 3390 cm^{-1} disappear and only sharp vibration peak at 3300 cm^{-1} was observed indicated the formation of the corresponding Schiff bases [32]. The formation of the Schiff bases were accompanied by the appearance of the C=N vibration peak at 1595 cm^{-1} (Fig. 3a).

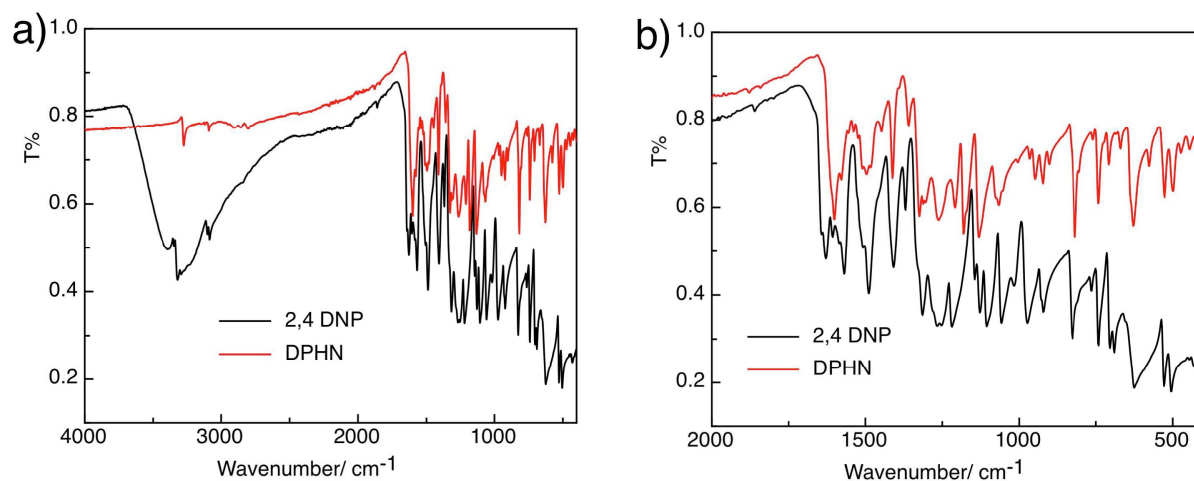


Fig. 3: FT-IR of a) 2,4-DNP and DPHN, b) magnified spectra 2,4-DNP and DPHN.

3.2 absorption spectra and solvent effect

The UV-Vis absorption spectra of 2,4-DNP derivatives are shown in Fig. 4. The synthesized Schiff bases gives an absorption peak in the 250-300 nm which assigned to the $\pi-\pi^*$ transition [27]. In addition, a strong and broad peak at 358, 370, 392, 424 for DPHB, DPHH, DPHS, and DPHN in ethanol was observed respectively (Table 1). The red shifted UV-Vis peak of 2,4-DNP derivatives was assigned to the $n-\pi^*$ transition. For example, the higher red shifted peak of DPHN at 424 nm in ethanol attributed to the intramolecular charge transfer (ICT) between the N-dimethylphenyl moiety (donor) and the 2,4 dinitrophenylhydrazine moiety (acceptor). The TD-DFT calculations were performed to determine the HOMO, LUMO frontier orbitals and the oscillator strength of the electronic transition (Fig. 5 and Table 1). The HOMO orbitals were distributed over the whole molecules, while the LUMO orbitals was situated over the 2,4-DNP moiety [27]. The energy gap gives an indication for important physical parameters such as stability and reactivity. Table 2 show that 2,4 DNP hydrazones have small energy gap that indicates the presence of small energy barrier for electron transfer transition. The red shifted peak in 2,4 DNP hydrazones was assigned to the HOMO \rightarrow LUMO transition (Fig. 5), which have the higher electronic transition and higher oscillator strength (Table 2). The calculated transition (TD-DFT) The calculated band gap

was in the order of DPHH > DPHS > DPHB > DPHN, which in accordance with the experimental absorption peak position the same order. The exceptional band gap decrease in DPHB could be attributed to the offset structure from linearity and the higher charge transfer to 2,4-DNP moiety (-0.25) compared to other derivatives (Table 2).

In order to investigate the solvent effect on the optical properties, the absorption spectra of 2,4-DNP hydrazone derivatives were monitored in different solvents (Fig. 4). The absorption spectra of the 2,4-DNP derivatives show significant change with the change in solvent polarity, particularly, in polar solvents. The absorption spectra were red shifted with the increase in the solvent polarity (Table 1) in DMF > ACN > MeOH > EtOH > CHCl₃. In order to confirm the stability of 2,4 DNP hydrazones in polar solvents, the TD-DFT were performed using self-consistent reaction field (SCRF) and polarized continuum model (PCM). The predicted absorption peaks along with the oscillator strength for the singlet-singlet transition are shown in Table 2. The results show that the ICT peak was red shifted from ethanol to DMF, which attributed to the increase of the solvent polarity.

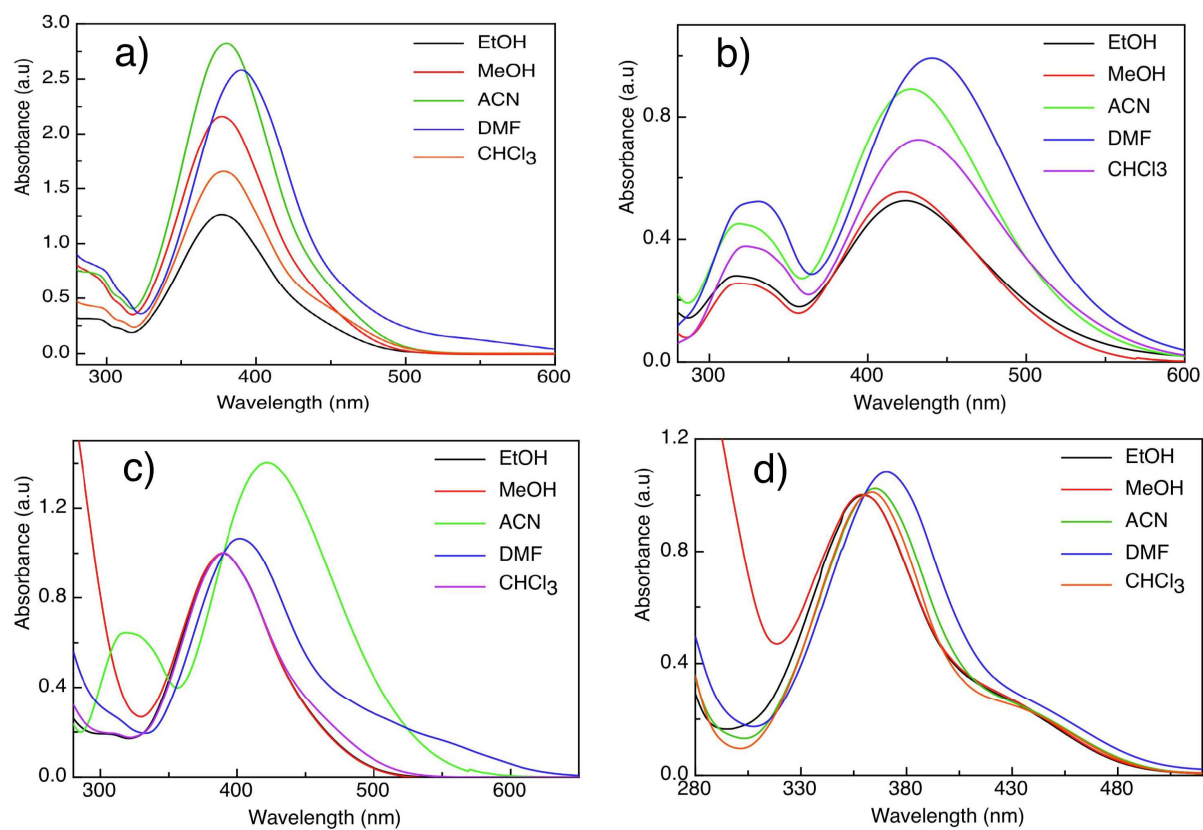


Fig. 4: Absorption spectra of 10 μm of a) DPHH, b) DPHN, c) DPHS, and d) DPHB in different solvents.

Table 1: Measured and calculated (TD-DFT) absorption spectra of 2,4 DNP hydrazone derivatives in different solvents (λ_{max} in nm).

	ϵ	DPHB		DPHH		DPHS		DPHN	
		Exp.	Calc.	Exp.	Calc.	Exp.	Calc.	Exp.	Calc.
DMF	37.22	372	378 (0.72) ^a	391	395 (0.65)	403	408 (0.74)	441	446 (0.81)
ACN	35.68	367		382		424		428.6	

MeOH	32.6	360		378		392		422	
EtOH	24.85	358	367.2 (0.63)	370	375 (0.64)	392	399 (0.74)	424	428 (0.84)
CHCl ₃	4.7	350		365		392		432	

^a Oscillator strength for the HOMO-LUMO transition

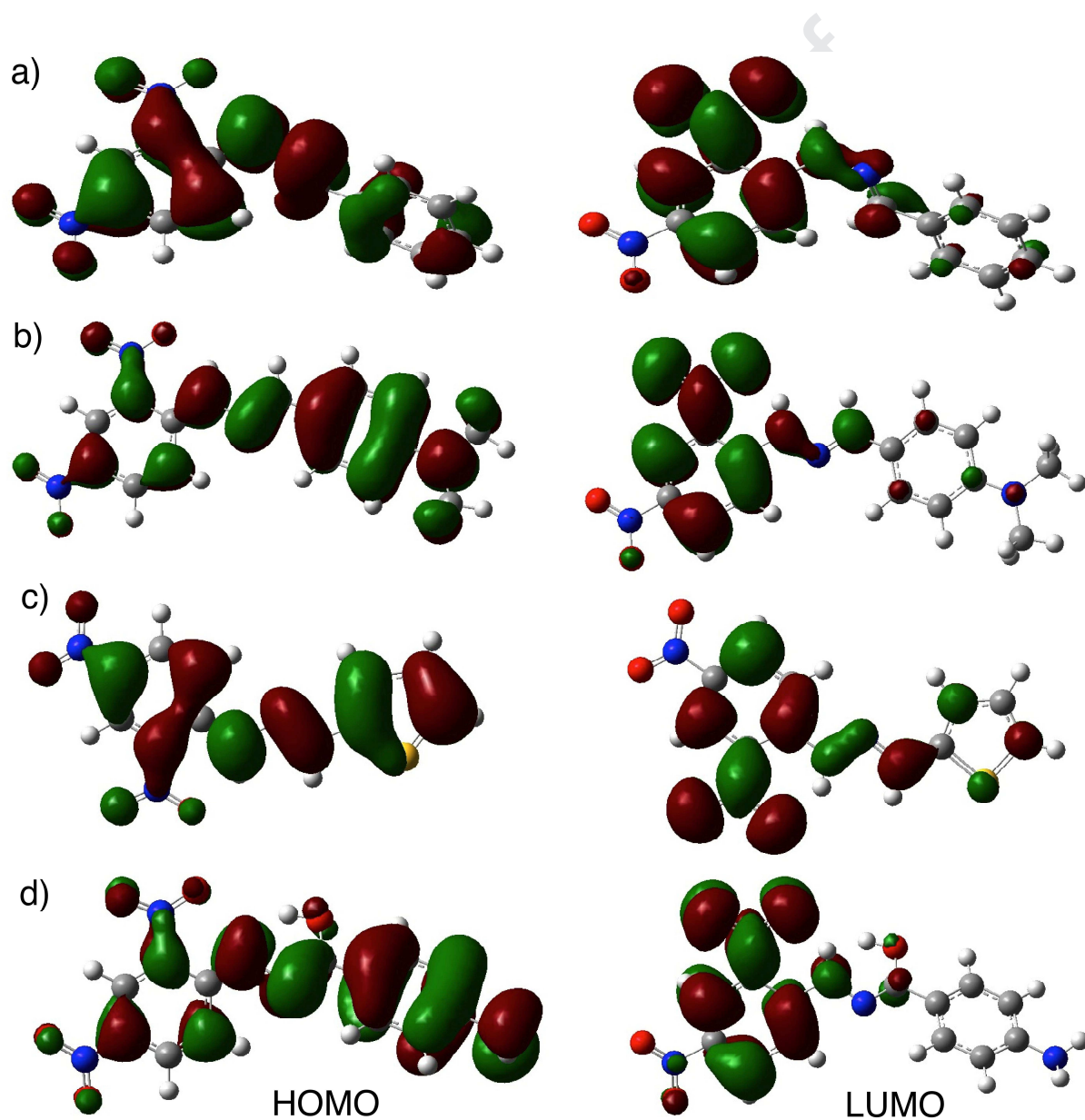


Fig. 5: calculated HOMO and LUMO orbital for the optimized structures of 2,4-DNP hydrazone derivatives a) DPHH, b) DPHN, c) DPHS, and d) DPHB calculated at B3lyp/6-311g(d,p).

3.3 Molecular Electrostatic potential of 2,4 DNP hydrazone derivatives

In order to investigate the reactivity of the 2,4 DNP hydrazone, the molecular electrostatic potentials (MEP) for the optimized compounds were calculated. MEP predicts the charge distribution over the molecule; the negative region is dominated by the high electron density and prone to an electrophilic attack or performs as electron donor sites. On the other hand, the positive region is an electron deficient region and prone to nucleophilic attack or perform as electron acceptor sites. The MEP of the 2,4 DNP hydrazone derivatives were performed at the optimized structure (B3lyp/6-311g(d,p)) (Fig. 6). The negative charge sites were situated on the NO₂ group of the 2,4 DNP moiety, while the positive sites were localized on the substituted aryl moiety.

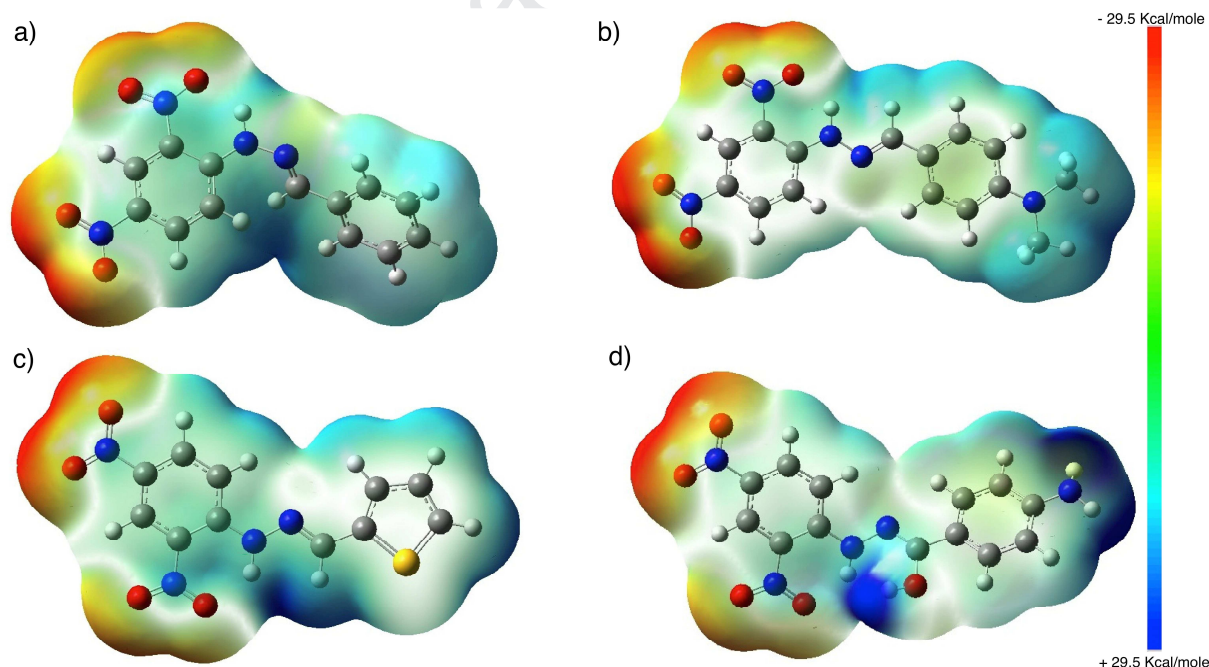


Fig. 6: Calculated molecular electrostatic potential of 2,4-DNP hydrazone derivatives a) DPHH, b) DPHN, c) DPHS, and d) DPHB calculated at B3lyp/6-311g(d,p).

3.4 Immobilization of hydrazone derivatives on *g*-C₃N₄ surface

In order to investigate the optical properties of the 2,4-DNP derivatives on the $g\text{-C}_3\text{N}_4$ surface, 5% from the DPHX compounds were added to the $g\text{-C}_3\text{N}_4$. The FT-IR spectrum of $g\text{-C}_3\text{N}_4$ gives a broad peak for the N-H group in the range $3100\text{-}3300\text{ cm}^{-1}$, which was broadens after the addition of hydrazone derivatives (Fig. 7a). Weak peaks in the $100\text{-}1200$ were observed due to the C-N stretching mode that confirm the successful integration of hydrazone derivatives into $g\text{-C}_3\text{N}_4$ structure [25]. The XRD diffraction of $g\text{-C}_3\text{N}_4$ shows two peaks at 13° and 27° for the in-plane structure and the interlayer stacking respectively (Fig.7b) [40]. Doping of the $g\text{-C}_3\text{N}_4$ with 5% of the DPHX derivatives did not change the peak position, however, the peaks were broaden that confirm the intercalation of the Schiff bases between the $g\text{-C}_3\text{N}_4$ layers [40]. The UV-vis absorption of DPHS shows a peak at 390 nm in ethanol solution. Upon addition of 3 mg/ml $g\text{-C}_3\text{N}_4$ to an ethanolic solution of DPHS, the UV-vis absorption spectra shows an enhanced absorption tail in the visible region in addition to the main peak at 390 nm (Fig. 7c).

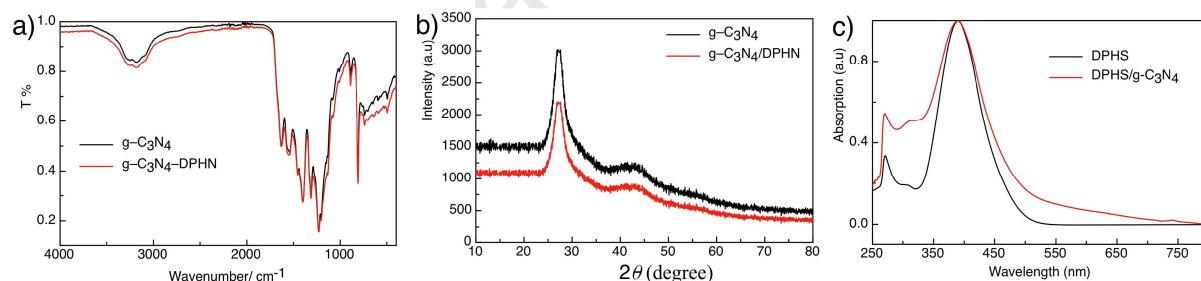


Fig. 7: a) FT-IR spectrum and b) XRD diffraction of $g\text{-C}_3\text{N}_4$ and $g\text{-C}_3\text{N}_4\text{-DPHN}$, c) absorption spectra of $10\ \mu\text{m}$ DPHS and $g\text{-C}_3\text{N}_4\text{/DPHS}$ in ethanol.

The emission spectra of 2,4-DNP derivatives show very low fluorescence peak at 470 nm. The low emission of the 2,4-DNP derivatives attributed to the internal photo-electron transfer (PET) from the aryl moiety to the 2,4-DNP moiety. On the other hand, $g\text{-C}_3\text{N}_4$ shows broad fluorescence peak at 456 nm ($\lambda_{\text{ex}} = 400\text{ nm}$), attributed to the fast electron/hole recombination process [41]. Upon immobilization of the 2,4-DNP derivatives on $g\text{-C}_3\text{N}_4$ surface, the

emission peak at 456 nm was decreased due to inhibition of electron/hole recombination process. For example, addition of 80 μM of PDHH to $\text{g-C}_3\text{N}_4$ decreases the emission intensity by 63% (Fig. 8a). The emission of $\text{g-C}_3\text{N}_4$ was red shifted with the addition of 2,4-DNP hydrazone derivatives (Fig. 8b), which ascribed to decreases of the band gap and existence of sub-band gap levels [41].

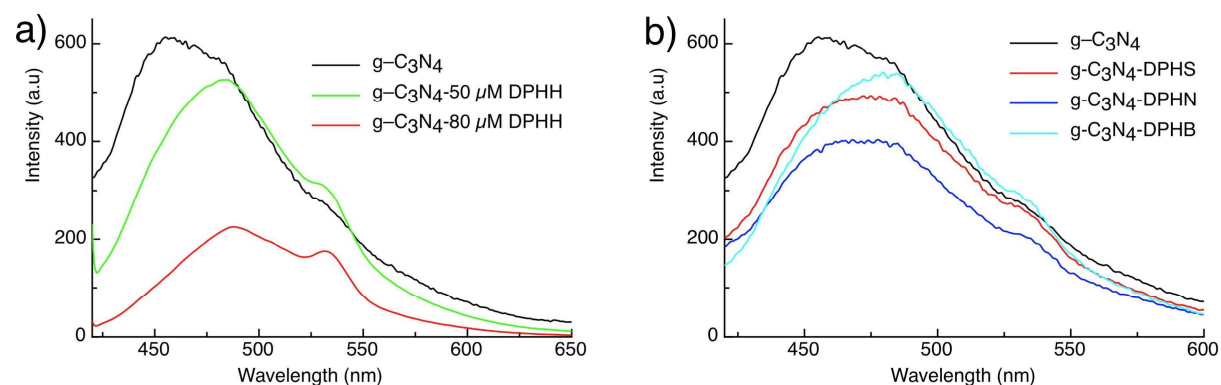


Fig. 8: Fluorescence ($\lambda_{\text{ex}} = 400 \text{ nm}$) of a) $\text{g-C}_3\text{N}_4$ with different concentration of DPHH and, b) $\text{g-C}_3\text{N}_4$ with different 2,4 DNP hydrazone derivatives in MeOH.

Fig.9a show the reflectance spectra of 5% 2,4 DNP derivatives deposited on $\text{g-C}_3\text{N}_4$. The spectrum shows the change of $\text{g-C}_3\text{N}_4$ reflectance with the 5% 2,4 DNP derivatives. The change in the band gap of $\text{g-C}_3\text{N}_4$ was calculated after the addition of 5% 2,4 DNP derivatives (Fig. 9b). The pristine $\text{g-C}_3\text{N}_4$ possesses band gap energy of 2.7 eV [42,43]. Table 2 shows that addition of 5% 2,4 DNP derivatives to $\text{g-C}_3\text{N}_4$ decreases the band gap from 2.71 to 2.62 eV with the addition of 5% DPHN [25]. The DFT calculations of DPHX/ $\text{g-C}_3\text{N}_4$ show the stabilizations of the composite by noncovalent interactions. The calculated energy gap at the optimized structures was used to corroborate the experimental data. The E_g of the optimized structures indicate the decrease of the $\text{g-C}_3\text{N}_4$ band gap with the addition of different hydrazone derivatives in the order $\text{DPHH} < \text{DPHS} < \text{DPHB} < \text{DPHN}$ (Table 2). This result is in accordance with the increase of the charge transferred from $\text{g-C}_3\text{N}_4$ to DPHX derivatives

(Table 2) that inhibit the electron/hole recombination [44]. In addition, the decrease in the band gap intensity increases with the increase of the DPHX light absorption in the visible region. Table 1 show that the absorption spectra of DPHN is more red shifted ($\lambda_{\max}= 441$ nm in DMF), which improve the light absorption of g-C₃N₄ and tune the band gap structure [25].

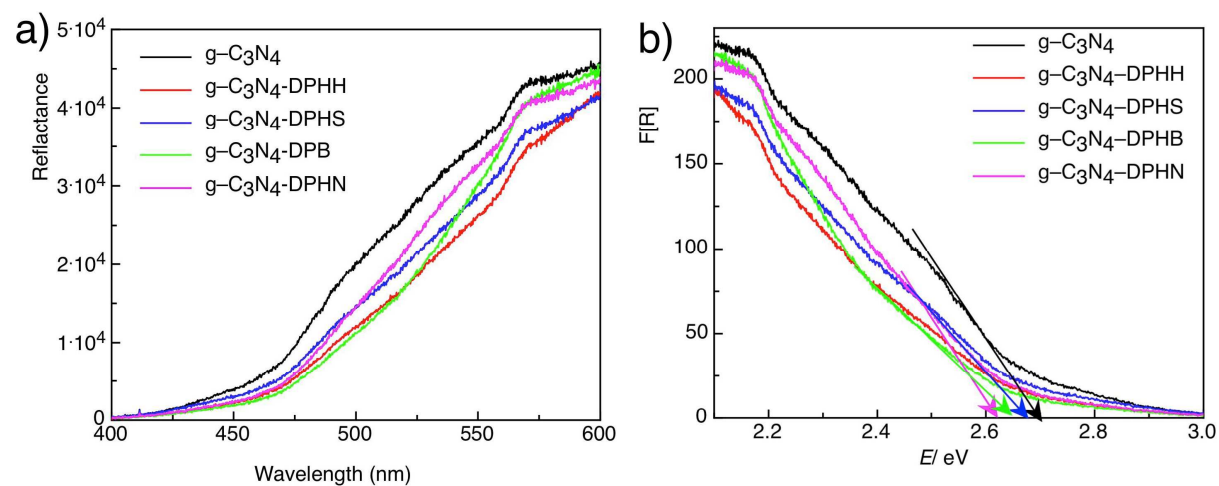


Fig. 9: a) reflectance spectra of g-C₃N₄ and 5% 2,4 DNP hydrazones, b) Diffuse reflectance of g-C₃N₄ and 2,4 DNP derivatives.

Table 2: Calculated HOMO, LUMO, energy gap (eV), electronic charge (C/e) on g-C₃N₄ at B3lyp/6-311g(d,p) and the measured band gap of the solid 2,4 DNP hydrazone derivatives.

	E_{HOMO}^a	E_{LUMO}^a	E_{gap}^a	Band gap	C/e
g-C ₃ N ₄	-6.70	-3.03	3.67	2.71	0
DPHH	-6.52	-2.98	3.54		
g-C ₃ N ₄ / 5%DPHH	-6.33	-2.94	3.39	2.70	0.04
DPHS	-6.31	-3.09	3.22		
g-C ₃ N ₄ / 5%DPHS	-6.12	-3.08	3.04	2.68	0.06
DPHB	-5.99	-2.95	3.04		
g-C ₃ N ₄ / %DPHB	-5.51	-3.22	2.29	2.65	0.07
DPHN	-5.59	-2.80	2.79		

g-C ₃ N ₄ / 5%DPHN	-5.43	-3.22	2.21	2.62	0.15
--	-------	-------	------	------	------

3.5 Analysis of Noncovalent Interactions (NCI)

Noncovalent interactions such as hydrogen bonding, halogen bonding, π - π interactions, and vdW forces were responsible for the assembly of molecular and supramolecular systems [45-48]. In order to investigate the nature of the molecular interactions between the 2,4-DNP derivatives with g-C₃N₄, NCI theory was used [35,49]. NCI distinguishes weak interactions as low electron density (ρ) and low reduced density gradients (RDG) areas. In NCI, the blue isosurface value indicate the presence of strong attractive interactions, while the green isosurface shows the presence of weak interactions such as vdW forces [35,50]. Analyzing the NCI results shows that the main forces between g-C₃N₄ and 2,4-DNP derivatives is the vdW forces (green isosurface) and hydrogen bonding (Fig. 10). The vdW forces appears at $-0.01 \text{ a.u.} < (\lambda_2)\rho > 0.01 \text{ a.u.}$ (Fig. 11). In addition, the RDG plot shows the presence of hydrogen bond (HB) at $-0.02 \text{ a.u.} < (\lambda_2)\rho > -0.01 \text{ a.u.}$, which ascribed to the intramolecular hydrogen bonding within the hydrazine derivatives (Fig. 11) and intermolecular hydrogen bonding in g-C₃N₄/2,4-DNP hydrazone derivatives.

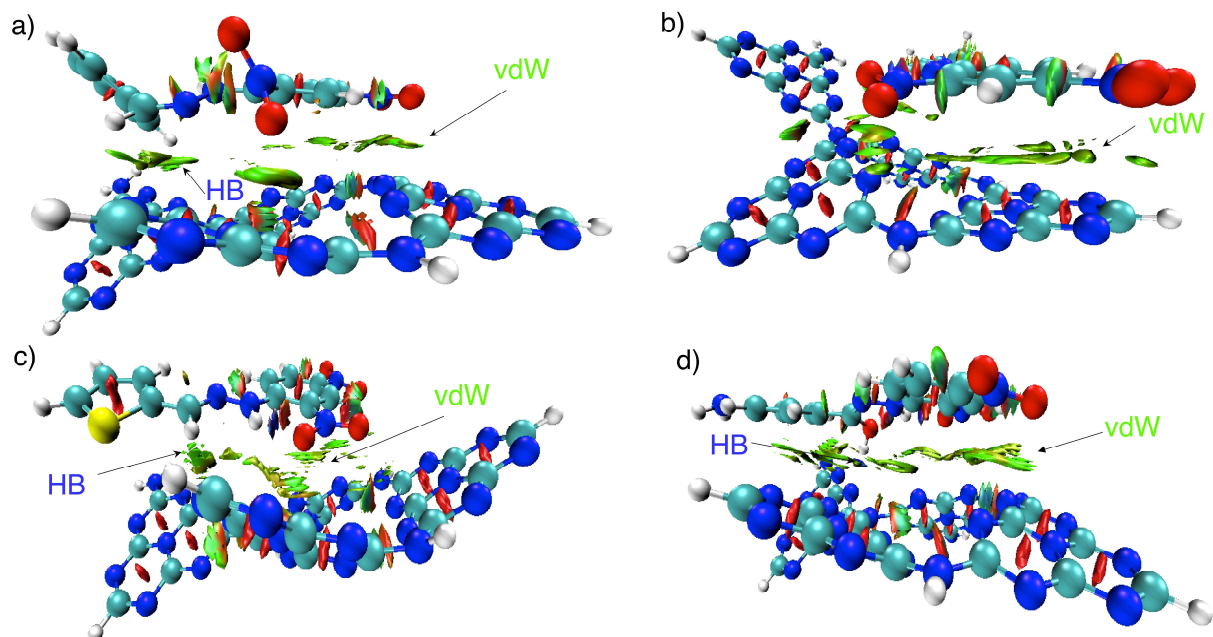


Fig. 10: Noncovalent interaction isosurface plot of a) DPHH, b) DPHN, c) DPHS, and d) DPHB

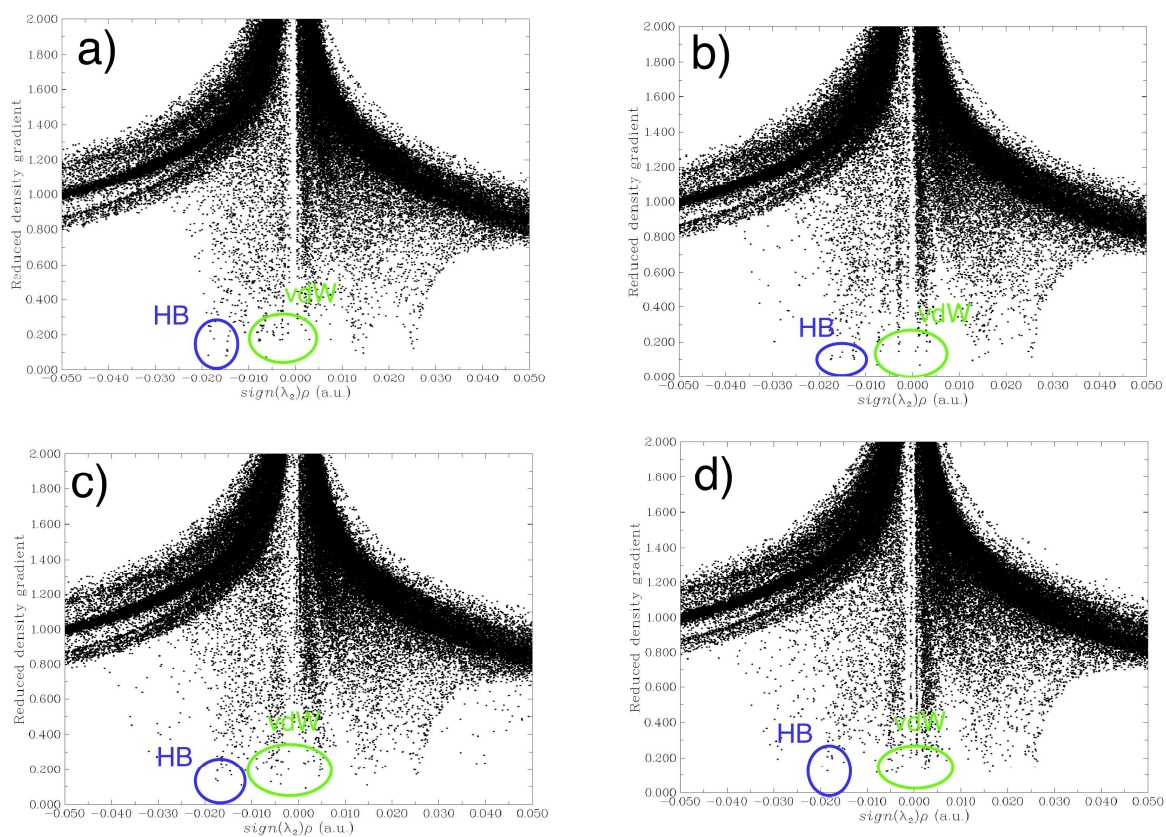


Fig. 11: NCI 2D plot of a) DPHH, b) DPHS, c) DPHN, and d) DPHB

The molecular interactions between $g\text{-C}_3\text{N}_4$ and 2,4-DNP derivatives were investigated in ethanol and DMF environments using the optimized structures at B3lyp/6-311g(d,p) level and PCM solvent model. Table 3 shows the relative binding energies of the $g\text{-C}_3\text{N}_4$ /DPHX and the corresponding charge transfer from $g\text{-C}_3\text{N}_4$ to DPHX derivatives. The calculated binding energy of the investigated complexes was higher in DMF than ethanol with the increase of the amount of the transferred charges in the same order. This indicates that the complexes are stabilized in the polar solvents, which could be attributed to the facile charge transfer inside the complexes in polar solvents.

Table 3: Relative binding energies (kcal/mole) of DPHX/ $g\text{-C}_3\text{N}_4$ in different solvents calculated at B3lyp/6-311g(d,p) level and PCM solvent model.

	EtOH	DMF
$g\text{-C}_3\text{N}_4$ /DPHH	-4.6 (0.06) ^a	-7.2 (0.015)
$g\text{-C}_3\text{N}_4$ /DPHS	-4.9 (0.08)	-8.1 (0.025)
$g\text{-C}_3\text{N}_4$ /DPHB	-5.4 (0.014)	-8.6 (0.030)
$g\text{-C}_3\text{N}_4$ /DPHN	-6.1 (0.020)	-8.2 (0.040)

^aData in parenthesis is the charge transferred from $g\text{-C}_3\text{N}_4$ to DPNX

4. Conclusion

Four hydrazone derivatives of 2,4 dinitrophenylhydrazine were synthesized and characterized using different spectroscopic techniques. The optical properties of the derivatives were investigated in different solvents. The UV-Vis absorption of the hydrazones were stabilized in polar solvents, which confirmed by the TD-DFT calculations. Immobilization of the hydrazone derivatives on $g\text{-C}_3\text{N}_4$ surface were stabilized by noncovalent interactions such as hydrogen bonding and vdW forces. The optical band gap of

g-C₃N₄ was decreased by doping of 5% of DPNX derivatives, which attributed to the extended absorption of the complexes in the visible region and facile charge immobilization.

Acknowledgment

The author thanks Taif University, Deanship of scientific research for financial support with project No.1/439/6061.

5. References

- [1] J. Liu, Y. Wang, J. Ma, Y. Peng, A. Wang, *J. Alloys Compd.* 783 (2019) 898.
- [2] V. Hasija, P. Raizada, A. Sudhaik, K. Sharma, A. Kumar, P. Singh, S.B. Jonnalagadda, V.K. Thakur, *Appl. Mater. Today* 15 (2019) 494.
- [3] V.N. Rao, N.L. Reddy, M.M. Kumari, K.K. Cheralathan, P. Ravi, M. Sathish, B. Neppolian, K.R. Reddy, N.P. Shetti, P. Prathap, T.M. Aminabhavi, M.V. Shankar, *J. Environ. Manage.* 248 (2019) 109246.
- [4] J. Hu, P. Zhang, W. An, L. Liu, Y. Liang, W. Cui, *Appl. Catal. B* 245 (2019) 130.
- [5] G. Ye, Z. Yu, Y. Li, L. Li, L. Song, L. Gu, X. Cao, *Water Res.* 157 (2019) 134.
- [6] G. Liao, Y. Gong, L. Zhang, H. Gao, G.-J. Yang, B. Fang, *Energy Environ. Sci.* 12 (2019) 2080.
- [7] V. Kumaravel, S. Mathew, J. Bartlett, S.C. Pillai, *Appl. Catal. B* 244 (2019) 1021.
- [8] A. Meng, L. Zhang, B. Cheng, J. Yu, *Adv. Mater.* 31 (2019) 1807660.
- [9] P. Zhang, H. Xiang, L. Tao, H. Dong, Y. Zhou, T.S. Hu, X. Chen, S. Liu, S. Wang, S. Garaj, *Nano Energy* 57 (2019) 535.
- [10] C. Hu, Z. Jiang, W. Zhou, M. Guo, T. Yu, X. Luo, C. Yuan, *J. Phys. Chem. Lett.* 10 (2019) 4763.
- [11] Q. Jin, Y. Shen, Y. Cai, L. Chu, Y. Zeng, *J. Hazard. Mater.* 381 (2020) 120934.
- [12] G. Zhang, G. Li, T. Heil, S. Zafeiratos, F. Lai, A. Savateev, M. Antonietti, X. Wang, *Angew. Chem.* 131 (2019) 3471.
- [13] L.M. Azofra, D.R. MacFarlane, C. Sun, *Phys. Chem. Chem. Phys.* 18 (2016) 18507.
- [14] M. Ghashghaee, Z. Azizi, M. Ghambarian, *Struct. Chem.* (2020) <https://doi.org/10.1007/s11224>.
- [15] A. Bafekry, C. Stampfl, B. Akgenc, M. Ghergherehchi, *Phys. Chem. Chem. Phys.* 22 (2020) 2249.
- [16] S. Sarikurt., F. Ersan, *Marmara fen bilim. derg.* 30 (2018) 383.
- [17] Y.Z. Abdullahi, T.L. Yoon, M.M. Halim, M.R. Hashim, T.L. Lim, *Solid State Commun.* 248 (2016) 144.
- [18] A. Bafekry, C. Stampfl, B. Akgenc, B. Mortazavi, M. Ghergherehchi, C.V. Nguyen, *Phys. Chem. Chem. Phys.* 22 (2020) 6418.
- [19] J. Qin, J. Huo, P. Zhang, J. Zeng, T. Wang, H. Zeng, *Nanoscale* 8 (2016) 2249.
- [20] H.S. El-Sheshtawy, H.M. El-Hosainy, K.R. Shoueir, I.M. El-Mehasseb, M. El-Kemary, *Appl Surf Sci.* 467-468 (2019) 268.
- [21] J. Xu, Y. Qi, W. Wang, L. Wang, *Int. J. Hydrogen Energ.* 44 (2019) 4114.
- [22] J. Ma, D. Huang, W. Zhang, J. Zou, Y. Kong, J. Zhu, S. Komarneni, *Chemosphere* 162 (2016) 269.
- [23] P. Zhang, T. Wang, H. Zeng, *Appl. Surf. Sci.* 391 (2017) 404.

- [24] X.-B. Qian, W. Peng, J.-H. Huang, *Mater. Res. Bull.* 102 (2018) 362.
- [25] H. Zhang, J. Lin, Z. Li, T. Li, X. Jia, X.-L. Wu, S. Hu, H. Lin, J. Chen, J. Zhu, *Catal. Sci. Technol.* 9 (2019) 502.
- [26] Z. Li, Y. Wu, G. Lu, *Appl. Catal. B* 188 (2016) 56.
- [27] N. Dege, M.S.H. Faizi, O.E. Dogan, E. Agar, I.A. Golenya, *Acta Crystallogr. E* 75 (2019) 770.
- [28] D.M. Gil, *J. Mol. Struct.* 1205 (2020) 127589.
- [29] H. Wang, Y. Li, S. Yang, H. Tian, Y. Liu, B. Sun, *J. Photochem. Photobiol. A* 377 (2019) 36.
- [30] X. Guo, S. Li, S. Mu, Y. Zhang, X. Liu, H. Zhang, *Spectrochim Acta. A Mol. Biomol. Spectrosc.* 226 (2020) 117625.
- [31] Y. Liu, F. Cao, H. Xiong, Y. Shen, M. Wang, *PLOS ONE* 11 (2016) e0163836.
- [32] A. Afkhami, M. Saber-Tehrani, H. Bagheri, *J. Hazard. Mater.* 181 (2010) 836.
- [33] P.P. Mukovoz, E.S. Dankovtseva, V.P. Mukovoz, P.A. Slepukhin, I.N. Ganebnykh, A.N. Sizontsov, E.A. Danilova, *Russ. J. Gen. Chem.* 89 (2019) 1.
- [34] M.J. Frisch, G.W. Trucks, H.B. Schlegel, G.E. Scuseria, M.A. Robb, J.R. Cheeseman, G. Scalmani, V. Barone, B. Mennucci, G.A.e.a. Petersson, (2009) Wallingford.
- [35] T. Lu, F. Chen, *J. Comput. Chem.* 33 (2012) 580.
- [36] W. Humphrey, A. Dalke, K. Schulten, *J. Mol. Graph.* 14 (1996) 33.
- [37] H.S. El-Sheshtawy, A.M. Abou Baker, *J. Mol. Struct.* 1067 (2014) 225.
- [38] J. Restrepo, C. Glidewell, N. Cubillán, Y. Alvarado, N. Dege, M. Morales-Toyo, *J. Mol. Struct.* 1177 (2019) 363.
- [39] R.M. Silverstein, F.X. Webster, *Spectrometric Identification of Organic Compounds*, Jon Wiley Sons. Inc., New York, 1963.
- [40] Z. Zhang, J. Huang, Q. Yuan, B. Dong, *Nanoscale* 6 (2014) 9250.
- [41] S. Li, C. Hu, Y. Peng, Z. Chen, *RSC Advances* 9 (2019) 32674.
- [42] S. Zuluaga, L.-H. Liu, N. Shafiq, S.M. Rupich, J.-F. Veyan, Y.J. Chabal, T. Thonhauser, *Phys. Chem. Chem. Phys.* 17 (2015) 957.
- [43] T. Giannakopoulou, I. Papailias, N. Todorova, N. Boukos, Y. Liu, J. Yu, C. Trapalis, *Chem. Eng. J.* 310 (2017) 571.
- [44] M. Ahmad, M.Y. Khan, S. Sadaf, S. Iqbal, F. Nawaz, J. Iqbal, *Mater. Res. Express* 6 (2019) 055050.
- [45] H.S. El-Sheshtawy, M.M. Ibrahim, I. El-Mehasseb, M. El-Kemary, *Spectrochim Acta. A Mol. Biomol. Spectrosc.* 143 (2015) 120.
- [46] H.S. El-Sheshtawy, H.M.A. Salman, M. El-Kemary, *Spectrochim Acta. A Mol. Biomol. Spectrosc.* 137 (2015) 442.
- [47] H.S. El-Sheshtawy, I. El-Mehasseb, *J. Mol. Struct.* 1147 (2017) 643.
- [48] H.S. El-Sheshtawy, M.M. Ibrahim, M.R.E. Aly, M. El-Kemary, *J. Mol. Liq.* 213 (2016) 82.
- [49] M.N. Shewale, D.N. Lande, S.P. Gejji, *J. Phys. Chem. A* 121 (2017) 288.
- [50] X. Zhang, X. Du, J. Song, J. Huang, *J. Phys. Org. Chem.* 33 (2020) e4016.

Highlights

- Synthesis, DFT calculations, and solvent effect of 2,4-DNP Derivatives.
- Polar solvents stabilize the absorption of 2,4-DNP Derivatives under visible light.
- The band gap of g-C₃N₄ nanosheet decreases by 2,4-DNP derivatives due to charge transfer and light absorption increasing.
- Noncovalent interactions stabilize the 2,4-Dinitrophenylhydrazone Derivatives/g-C₃N₄ composite.

Conflict of interest: the author declare no conflict of interest

Journal Pre-proof